Evaluating the Retreat, Stabilization, and Regrowth of Crane Glacier against Marine Ice Cliff Process Models

C. Needell[1] and N. Holschuh[1*]

[1]Department of Geology, Amherst College, Amherst, MA, USA

[*]Corresponding author: Nicholas Holschuh (nholschuh@amherst.edu)

Key Points (must be < 140 characters):

- Unstable, brittle retreat of Crane Glacier after the collapse of the Larsen B Ice Shelf occurred in mostly floating ice.
- Crane's retreat into a narrow fjord and sea-ice growth re-established buttressing stresses and arrested terminus retreat.
- Cliff failure may have occurred during the last phase of retreat, only consistent with models assuming heavily damaged ice.

Abstract

The fastest projected rates of sea level rise appear in models which include "the marine ice cliff instability (MICI)," a hypothesized but mostly unobserved process defined by rapid, brittle failure of terminal ice cliffs that outpaces viscous relaxation and ice-shelf formation. The response of Crane Glacier to the Larsen B Ice Shelf collapse has been invoked as observational evidence of this process, but limited data coverage in space and time has limited our ability to meaningfully refine our understanding of cliff failure processes using that event. Updates to Crane's subglacial topography show that much of its terminus retreat occurred in floating, not grounded ice, but its retreat, arrest, and regrowth over the last decade indicate brittle (not viscous) processes dominated during the 2 years following ice shelf collapse. If retreat occurred by cliff failure, maximum cliff heights would have been 111 m, consistent with process models that incorporate damaged ice.

Plain Language Summary

The behavior of Antarctic glaciers will largely determine the pace and magnitude of future sea level rise. But the projections made by ice sheet models are uncertain, in part due to the uncertain response of Antarctica to the loss of its floating ice shelves. It has been hypothesized that ice shelf breakup could trigger a self-sustaining mechanism of ice loss whereby ice cliffs collapse under their own weight. This idea is controversial because it has not been unambiguously observed in modern glacier systems, in part because the modern ice sheet margins are geometrically different from the margins that will exist during West Antarctic deglaciation. Some claim that Crane Glacier, located on the Antarctic Peninsula, has shown behavior consistent with this process, but we show here that much of the observed ice loss likely occurred by more established "calving" processes. If cliff failure did occur, existing models require damaged ice to reproduce Crane's behavior.

1 Introduction

The West Antarctic Ice Sheet (WAIS) is bounded by floating ice shelves, which play a critical role in buttressing ice stored in the continental interior (Dupont & Alley, 2005; Weertman, 1974). Ice shelves respond to atmospheric and ocean forcing, on average leading to acceleration and enhanced ice discharge to the ocean today (Pritchard et al., 2012). While ice shelf change over the early 21^{st} century has been dominated by ocean driven melt from below, the rapid disintegration of the Larsen B Ice Shelf (LBIS) by surface melt and ice-shelf hydrofracture has demonstrated that other modes of failure are possible (Glasser & Scambos, 2008), leading to a range of studies about the future of Antarctic ice shelves subject to a warmer atmosphere (Bell et al., 2018; Kingslake et al., 2017; Lai et al., 2020).

To accurately project the rates of future sea level rise (SLR), ice sheet models must capture the rate limiting processes. The delivery of ice to the ocean by glacier sliding is the rate limiting process for most ice sheet models, and thus much work is focused on improving both our theoretical understanding of the physics of sliding (Helanow et al., 2020; Zoet & Iverson, 2020) and our empirical methods for inferring the material properties governing sliding (Joughin et al., 2019; Riel et al., 2021). But in a world where rapid ice-shelf breakup is common and glacier termini sit in the unconfined basins of the WAIS interior, brittle processes may control the rate at which ice mass is lost and sea level rises.

The "marine ice cliff instability (MICI)" is the idea that self-sustaining retreat by brittle failure may dominate the deglaciation of WAIS. The inclusion of MICI into models of sea level rise results in an Antarctic SLR eight times the values predicted by models that do not include it by 2100 (Bulthuis et al., 2019; DeConto & Pollard, 2016; Golledge et al., 2019). While it is not the only source of spread in ice sheet projections, MICI does represent the largest source of uncertainty (Fox-Kemper et al., 2021).

Recent models built from physics first principles (Parizek et al., 2019; Clerc et al., 2019; Bassis et al., 2021; Schlemm et al., 2021; Crawford et al., 2021) support MICI's theoretical validity, but the modes and thresholds for failure differ across them. Underlying every model of cliff failure is the fracture toughness of ice, a critical but uncertain property controlled by the damage experienced by any given ice parcel (Borstad et al., 2012; Lhermitte et al., 2020; Mobasher et al., 2016). In addition, the height of subaerial ice cliffs that form after ice shelf collapse, the glacier geometry (Parizek et al., 2019; Bassis et al., 2021; Crawford et al., 2021), upstream velocity (Bassis et al., 2021; Crawford et al., 2021), and bed topography (Schlemm et al., 2021) have all been raised as essential controls on system behavior. Without observations of failure to refine our understanding of cliff dynamics, ice-sheet wide models rely heavily on process models of ice cliff failure to justify MICI's inclusion and potential parameterization.

There are few geological or geophysical observations capable of improving our understanding of ice cliff dynamics. The paleo-sea-level record may provide

indirect evidence of MICI; during several periods in Earth's history, ice sheet models have difficulty reproducing the observed rapid sea level rise without it (Wise et al., 2016), but there is disagreement in the literature about whether MICI is truly required to explain historical Antarctic ice loss (Edwards et al., 2019). The Intergovernmental Panel on Climate Change (IPCC) names Crane Glacier's response to the Larsen B Ice Shelf (LBIS) collapse as the only potential evidence for MICI behavior in the satellite record (Oppenheimer et al., 2019). Crane Glacier has significantly influenced community thinking about MICI, with its post-LBIS-collapse ice wastage rate used to constrain some parameterizations of cliff failure in continental scale modeling (DeConto and Pollard, 2016). But our knowledge of Crane Glacier's geometry and behavior following the LBIS collapse is limited by sparse geophysical data, challenging evaluation of whether MICI style cliff failure occured.

By both identifying what we do know and what we cannot know based on the data that are available, we can more precisely use Crane Glacier's behavior following the LBIS collapse event to refine our understanding of ice cliff failure. In this work, we use geophysical data to improve our understanding of both the rate and mechanisms for glacier terminus retreat. Finally, retreat behavior can be evaluated against process models, to both identify whether or not cliff failure was theoretically possible at Crane, and if so, what unknown model parameters must be for failure to occur there.

2 Observational Data at Crane Glacier

To use Crane Glacier as a tool for evaluating ice cliff models, we must do three things:

1. Constrain the rates of retreat, the glacier geometry (with a focus on terminus height), and the grounding line position through time.
2. Show that brittle processes governed Crane's retreat behavior after the LBIS collapse.
3. Infer the floatation state of the glacier terminus through time.

All three of these objectives are challenging. Brittle processes play out on very short timescales (from minutes to days) not captured by the recurrence interval of satellite observations. In addition, ice penetrating radar data collected over Crane Glacier before the LBIS collapse failed to clearly capture the ice bottom geometry, leaving a poorly constrained ice thickness profile, grounding line position, and terminus height at the time of collapse. But by revisiting the question of Crane Glacier's response to the LBIS collapse 20 years later, this study benefits from the following: marine geophysical data that captured the sea-floor morphology at the 2002 grounding line, additional aerogeophysical data capable of improving our knowledge of the upstream glacier geometry, and surface elevation observations that capture the return to an advanced state in the decades following collapse. These data allow us to better constrain the floatation state of the glacier terminus through time, an important factor given

that modes of cliff failure depend on the basal stress state of the system. Additionally, these data allow us to refine estimates of retreat rates and potentially narrow the range of thresholds (defined by current process models) that limit brittle failure.

1. **Surface Topography and Ice Velocity**

Glacier behavior before and after LBIS collapse is best characterized by altimetry and velocity time-series data (Figures 1, 2). Surface elevation data were collected along the centerline of Crane Glacier by Pre-IceBridge and IceBridge campaigns (Blair et al., 2018; Studinger, 2014; Thomas & Studinger, 2010); these form the primary basis for our analysis. Satellite radar altimeters (including Cryosat-2) suffer from reduced vertical accuracy in the high slope regions of the peninsula (Fang Wang et al., 2015), and while satellite laser altimeters (including ICESat and ICESat-2) capture surface elevation with high spatial precision, their sampling is limited by cloud-cover in the peninsula and track orientation and spacing in the region. Here, we use ICESat-2 ATL06 data to calibrate photogrammetric DEM's produced from Maxar stereopairs to extend the altimtery record through 2021.

There is uncertainty in the effective ice thickness at Crane in 2002 due to uncertainty in the firn air content (FAC) there (which reduces mass in the ice column, leading to stresses comparable to a shorter ice cliff than measured). The GSFC-FDMv1.1 model predicts 14 to 15 m of FAC near the Crane terminus and its upstream catchment (Medley et al., 2020; Figure S1), in contrast with the 0 m FAC observed on the LBIS immediately before its collapse (Holland et al., 2011). The GSFC-FDMv1.1 modeled FAC agrees with in-situ observations over the Larsen C (Ashmore et al., 2017), supporting model accuracy. We present both the conservative (observed height – 15 m) and maximum cliff heights (observed height assuming no FAC).

In addition to the altimetry record, MEaSUREs (Mouginot et al., 2017) and ITS_LIVE velocity data (Gardner et al., 2019) are used to characterize the evolving flow field of Crane Glacier after LBIS collapse.

2.2 Subglacial Topography and Floatation Criteria

Crane Glacier's bed elevation was refined by a marine geophysical survey conducted in the Larsen B Inlet in 2006 (Rebesco et al., 2014), which captured the bed over which the Crane terminus retreated. Radar campaigns designed to capture ice-bottom elevations in the currently glaciated regions were flown as part of NASA's Operation IceBridge from 2009 – 2017, but because of the narrow fjords and complex topography of the Antarctic Peninsula, those data suffer from significant off-axis clutter, resulting in an ambiguous basal reflector and an unknown ice thickness profile. We use the stack of all available radar data, compared with the multibeam swath bathymetry, to derive a range of reasonable bed elevations for the glacier interior (Figure S2, S3).

Monitoring the grounding line position and qunatifying the stress imbalance

at a marine ice cliff (and therefore its failure likelihood) requires knowledge of the ice thickness relative to the floatation thickness (the minimum ice thickness required to ground the ice bottom on the sea floor). With knowledge of the density of ice (ρ_i= 917 kg/m^3) the density of sea water (ρ_{sw}= 1027 kg/m^3), and the sea-floor elevation relative to the sea surface (b), the ice height at floatation (h_f) can be calculated by:

$$h_f = b\left(1 - \frac{\rho_{\text{sw}}}{\rho_i}\right)$$

Ultimately, we derive floatation heights from the radar data, multi-beam bathymetry, and estimates of the tidal state from sea-surface altimetry. This can be compared to the measured, firn air corrected surface elevation to estimate the grounding line position and grounding line evolution. Variability in the bed topography across-flow affects our estimate of the grounding zone position. To account for this, we calculate the floatation thickness using a range of ocean bottom elevations, sampling +/- 100 m orthogonal to the central flowline (Figure 1B).

2.3 The Imagery Record of Terminus Position and Sea Ice Cover

Due to infrequent collection of altimetry data over Crane immediately after the LBIS collapse, Landsat imagery was used to further constrain the timing of terminus retreat between 2002-2004. Landsat imagery also reveals the development of land-fast sea ice in the Crane Fjord in 2011 (Figure S4).

3 Retreat, Stabilization, and Regrowth of Crane Glacier

Remote sensing observations collected around the collapse event have been thoroughly discussed in the literature. Ice shelf retreat and thinning preceded the rapid collapse of the LBIS in February to March of 2002 (Glasser and Scambos, 2008). After collapse, the local buttressing stress at Crane Glacier's grounding line decreased by 30% (De Rydt et al., 2015). Crane Glacier showed little change immediately post-collapse in 2002 (Scambos, 2004), followed by accelerated ice loss from 2003-2007 (Scambos et al., 2011), and a slow deceleration of ice loss from 2008-2013 (Wuite et al., 2015).

The MICI hypothesis, invoked for Crane, is predicated on the idea that rates of brittle failure (and the resulting terminus retreat) outpace the ability of Crane to viscously thin. Below, we reframe and extend the observational record of Crane Glacier from 2002-2021 to highlight three distinct periods with the MICI hypothesis in mind: the initiation of brittle failure and rapid terminus retreat, the stabilization of the glacier terminus, and the regrowth and return to glacier equilibrium with the modern climate. We argue these data show (a) the geometric conditions under which brittle failure activates and deactivates for this system, and (b) the disequilibrium behavior of Crane Glacier during retreat, showing hysteresis in its response as it returns to an advanced configuration within the modern climate.

3.1 Period 1: Retreat (2002-2004)

From 2002-2004, rapid terminus retreat of over 9.5 km occured (Figure 2). During this period, the glacier thinned by 60.9 m at the location of the post-collapse ice front. Refinement to both our knowledge of the timing of retreat and the nature of the glacier terminus through time (was it floating or grounded?) would allow us to fully characterize the retreat processes. But because of the spatially and temporally sparse data available, questions about these two aspects of the system have proliferated in discussions of Crane in the literature.

Satellite-derived, pre-LBIS collapse grounding line positions do not agree with field evidence for the grounding line inferred from the sea-floor sedimentary record (Rebesco et al., 2014). Satellite data place the pre-collapse grounding line near the opening of the fjord (Rack and Rott, 2004), implying that most of the ice in Crane Glacier's narrow embayment was grounded before the LBIS collapse, and that the full extent of retreat observed from 2002-2004 occurred by failure of a grounded ice cliff. Radiocarbon-dated sediment cores suggest the pre-collapse grounding line was located much further inland of the fjord opening (Rebesco et al., 2014). This means that a substantial portion of the initial terminus retreat occurred in ice that was at or below floatation thickness (Figure 1B).

While the majority of the Larsen B collapsed during February and March of 2002, Landsat imagery from March of 2004 shows a glacier terminus that still had not retreated beyond the updated 2002 grounding line (Figure 2). That floating ice gradually reduced in extent until its final removal. Based on the elevation profile collected in November 2002 and the magnitude of thinning that is observed between 2002 and 2004, the final breakup of the remnant ice shelf occurred sometime after March 2004.

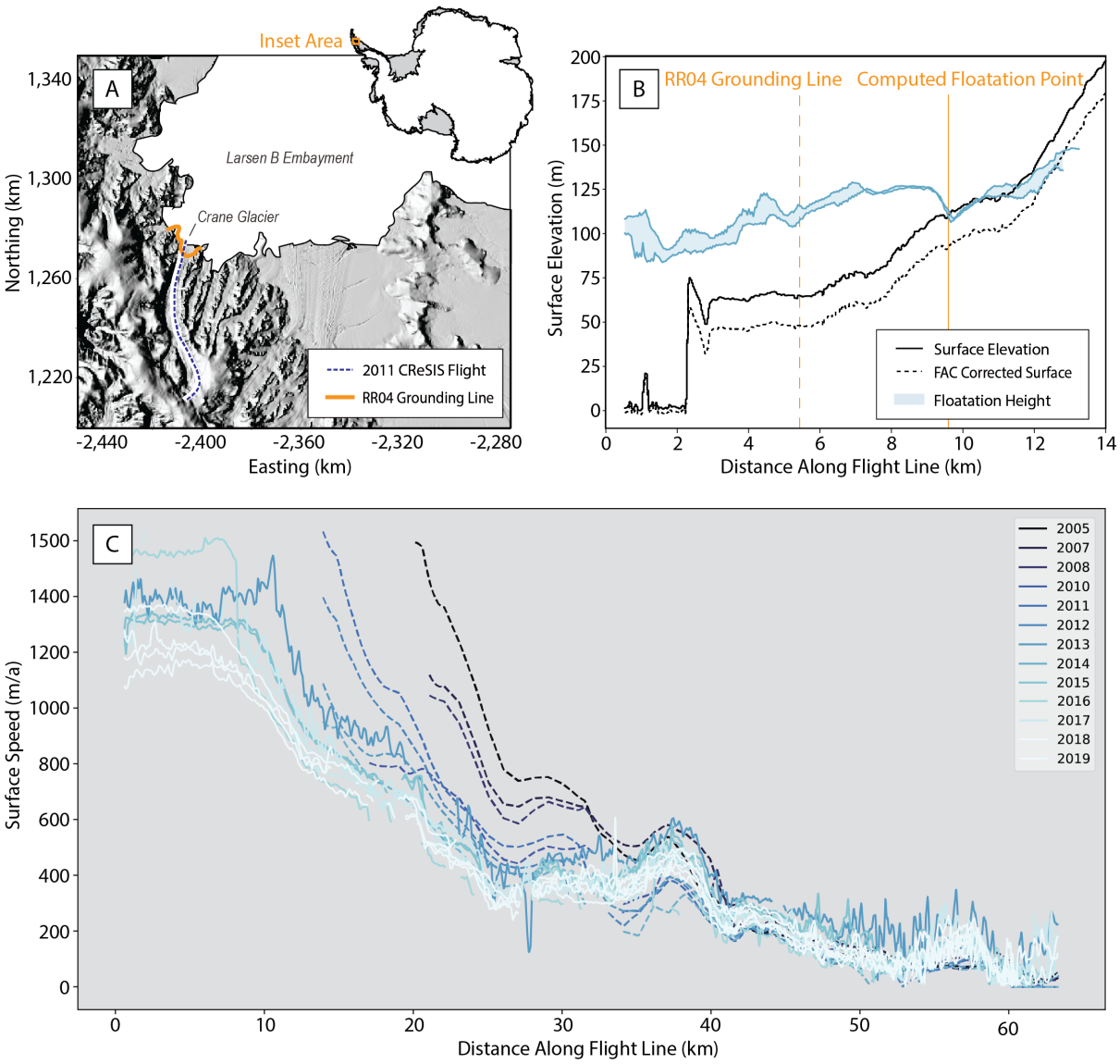

Figure 1. Crane Glacier's (a) location, (b) floatation state, and (c) ice velocity through time. (a) Hillshade map of the Larsen B Ice Shelf region, showing the 2011 CReSIS flight line (dashed blue, which we use as our central flowline) and an early, satellite-derived estimate of the 2002 grounding line (Rack and Rott, 2004; "RR04"; orange). (b) Range of floatation heights and ice surface elevations in November 2002, suggesting that the 2002 grounding line was situated 4 km inland of the RR04 grounding line. (c) ITS_LIVE (solid) and MEaSUREs (dashed) ice velocity from 2005-2019.

During the following 9 month period, the glacier experienced 4.7 km of terminus retreat, beginning 1 km down-flow of the updated 2002 grounding line and halting at the 2004 terminus. Thus, 3.7 km of this ice may have been grounded in 2002 (Figure 2). If grounded ice cliff failure occurred at Crane, it must have happened during this time window, which limits the maximum duration of cliff failure to the final stage of retreat, or 9 months. While there are no direct observations of an extant ice cliff during that period, the first ice cliff that could have formed (at the 2002 grounding line position) would have existed with a height of 111 m (Figure 1). Mass wastage by cliff failure during this (include both the ice resupplied to the terminus by ice flow in the 9 month period [1200 m, given ice velocities upwards of 1600 m/a] and the grounded ice loss) implies minimum failure rates of ~5.9 km in 9 months, or 7.9 km/a.

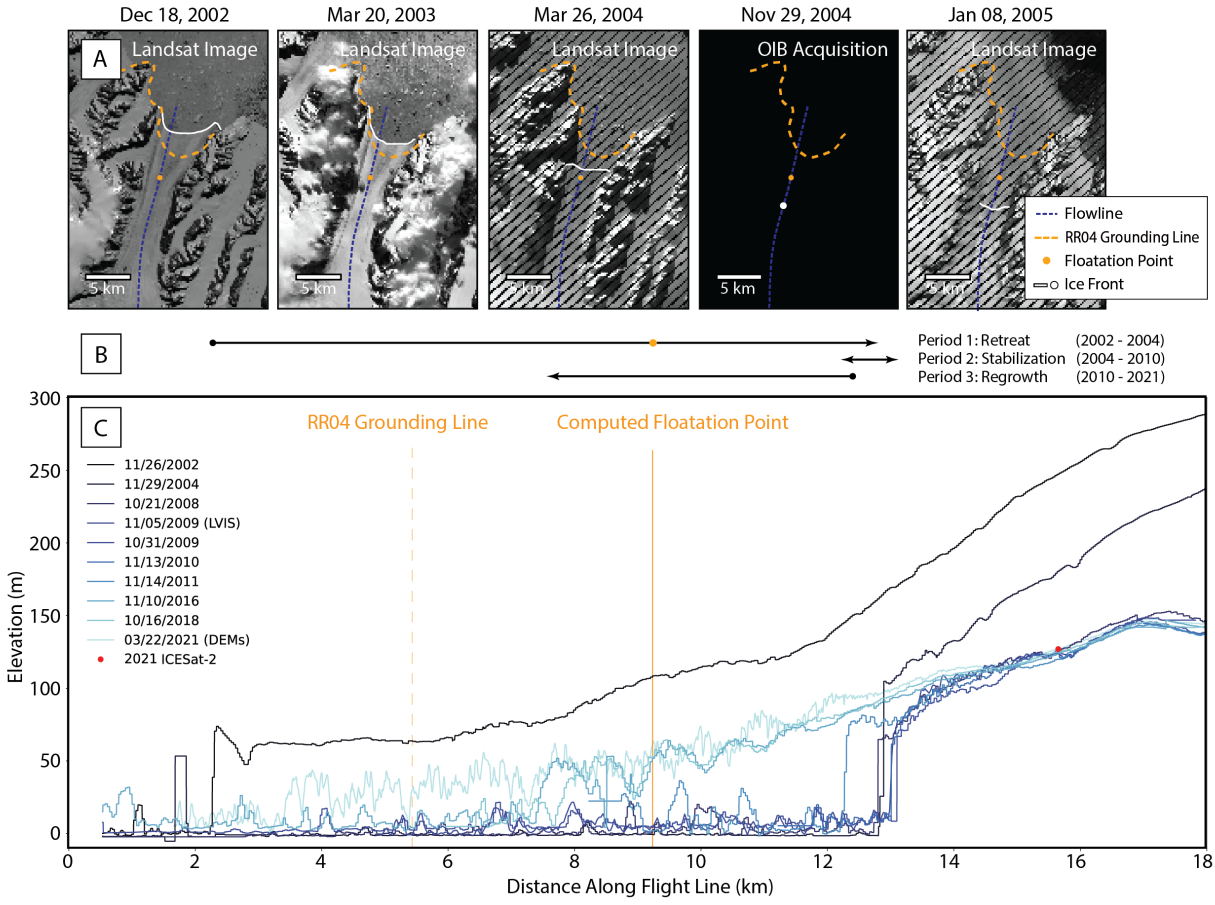

Figure 2. Data used to constrain timing of terminus retreat. (a) Landsat images of the Crane terminus, with manually-identified ice fronts (white), the RR04 grounding line (orange), and the calculated 2002 floatation point (orange)

shown. The ice front first retreated beyond the floatation-derived grounded point by November 2004. (b) Terminus evolution through time, corresponding to the (c) altimetry record of near-terminus surface elevation, collected using NASA's ATM and LVIS altimeters (2002-2018), and generated from ICESat-2-calibrated (red point) photogrammetric DEMs produced from Maxar stereopairs (2021).

3.2 Period 2: Stabilization (November 2004-2010)

By November 2004, the terminus of Crane Glacier had ceased its retreat 9.5 km upstream of its November 2002 terminus. The stress conditions there must have defined the threshold for brittle failure of the system – the terminus was unable to retreat further, but brittle failure continued there for the following six years, as the terminus position fluctuated by less than 0.5 km along the central flowline during that period. Meanwhile, the system adjusted to the large mass-disequilibrium by thinning upstream (Figure S5), reducing the driving stress and slowing its flow speed. This period saw an average thickness change of -16.3 m/a (0-15 km from the terminus) and a maximum velocity change of approximately -237.5 m/a^2, which occurred between 2005-2007 (0-20 km from the terminus).

3.3 Period 3: Regrowth (2010-2021)

From 2010-present, Crane's terminus has advanced and slowed. Additionally, the main trunk of Crane has thickened, while its tributaries have thinned since the launch of ICESat-2 in 2018 (Figure S5). From 2010-2011, the terminus advanced by 0.45 km. Limited elevation data were collected along Crane's flowline between 2012-2015, but surface elevation data from 2016-2018 capture an active calving front. This new terminus position, approximately 1.25 km downstream of the 2010 terminus, has remained stable since. Crane Glacier's near-terminus surface elevation increased by approximately 5 m/a over this 11 year period, as captured by ICESat-2 calibrated Maxar stereo-DEMs from 2019-2021 (Figures 2, S5). This thickening represents a redistribution of mass from the tributaries, where ICESat-2 data shows thinning of approximately 5 m/year from 2019-2021.

4 Discussion

4.1 Evaluating the Retreat Behavior of Crane Glacier

Without observations during the 9 month retreat window, there is no direct evidence of ice cliff failure at Crane Glacier. But there is indirect evidence that cliff failure may have occurred. The first and most often invoked evidence of cliff failure is the rapid rate of terminus retreat observed shortly after the LBIS collapse. Initial estimates of retreat assumed that at least 7.5 of the 9.5 km flowline was grounded (based on the satellite derived grounding line), which required a cliff failure rate of 5.4 km/a during the November 2002 – November 2004 period. With the updated grounding line, we show that only 3.7 km of terminus retreat could have occurred by grounded cliff failure during that 9 month window.

Crane's failure rate of 7.9 km/a represented an increase of its pre-collapse ice shelf calving rate (Alley et al., 2008), but wastage rates greater than 11 km/a have been recently observed elsewhere on the WAIS (Milillo et al., 2022), and at Jakobshavn and Helheim Glaciers in Greenland, whose velocities exceed 17 km/a (Joughin et al., 2014) and 11 km/a (Howat et al., 2005), respectively. However, the calving rates at Jakobshavn and Helheim, in part, accommodate their high terminus velocities (9,400 to 15,400 m/a faster than the terminus of Crane), which is an important qualitative difference between these systems and Crane. As such, the retreat rate observed at Crane does not fall outside of the range experienced by floating systems elsewhere in Antarctica and Greenland, but is anamolous for a glacier flowing only 1600 m/a at its terminus.

The second line of indirect evidence supporting cliff failure is the unstable nature of the retreat. Under stable retreat conditions, external forcing that reduces the back-stress at the terminus of a glacier (i.e., the breakup of the LBIS) would lead to glacier speed-up, which induces a mass imbalance that persists until viscous processes thin the system to a new stress- and mass-balance equilibrium profile. As we observed at Crane, brittle processes occurred faster than viscous thinning could adjust the system. Despite the fact that external forcing (the breakup of the LBIS) had ceased, terminus retreat continued off and on over a 2 year period, with a rapid final phase of retreat occurring where the ice had been clearly grounded in 2002. Brittle failure persisted until its new terminal stress state inhibited further retreat. Then, viscous processes dominated, the system thinned, and and the terminus advanced in its thinner state, leading to the formation of a new stable ice-shelf that extends into the Crane Glacier fjord.

Many conditions are known to inhibit cliff failure, including narrowing of the fjord, development of sea-ice in the fjord which can apply sufficient backstress to stabilize the cliff, retreat into thinner ice along a prograde slope, or retreat into ice that is not preconditioned for failure by crevassing or other processes that induce damage. In summer 2011, perennial landfast sea ice that formed in Crane Glacier's embayment (Figure S4) likely enabled the growth of an ice shelf, consistent with models of sea ice backstress (Robel, 2017) and documented sea-ice circulation patterns in the region (Christie et al., 2022). The reestablishment of a floating ice shelf facilitated Crane Glacier's recent thickening and velocity decrease.

Thus, we see 9.5 km of retreat by brittle processes, including potentially 3.7 km of terminus retreat by grounded cliff failure at Crane Glacier. With this established, the mechanisms for failure can be evaluated using the rapidly developing models used to understand ice cliff processes.

4.2 Evaluating Crane Retreat against Process Models

Models of ice cliff failure each have a stability threshold, defining the boundary between configurations that enable brittle collapse and those in which cliffs are stable and glaciers will thin and evolve by viscous processes. We can evaluate the behavior of Crane against published ice cliff process models (Clerc et al.,

2019; Bassis et al., 2021; Crawford et al., 2021; Parizek et al., 2019) in addition to earlier parameterizations of MICI (Bassis and Walker, 2012; DeConto and Pollard, 2016).

Although all models examined require an initially grounded cliff before the onset of MICI, a number of mechanisms exist under the "cliff failure" umbrella, including: fracture-induced full-thickness iceberg detachment (Bassis et al., 2021); initial slumping followed by buoyancy-driven retrogressive block rotation (Parizek et al., 2019; Bassis et al., 2021; Crawford et al., 2021); and forward block rotation resulting from surface crevassing (Crawford et al., 2021). While the stress-state at the water-line is the dominant control, stresses and velocities near the base of the glacier are sensitive to the floatation conditions. To compare with published models, claims of cliff failure at Crane rely on it being grounded, which could be the case for 3.7 km of its retreat in 2004.

Using nominal (undamaged) ice, process models require greater cliff heights (Bassis and Walker, 2012; Parizek et al., 2019; Clerc et al., 2019; Crawford et al., 2021) faster timescales of ice shelf collapse (Clerc et al., 2019), or a more extreme ice cliff gradient and bed slope (Bassis et al., 2021) than we observe at Crane Glacier to enable unstable retreat (Figure 3). When ice is treated as weak or damaged, all process models predict that MICI could occur at some point along Crane Glacier's trajectory of retreat between 2002-2004. This suggests that process models might more accurately predict MICI initiation if they consider weak ice as a realistic scenario, rather than an extreme one.

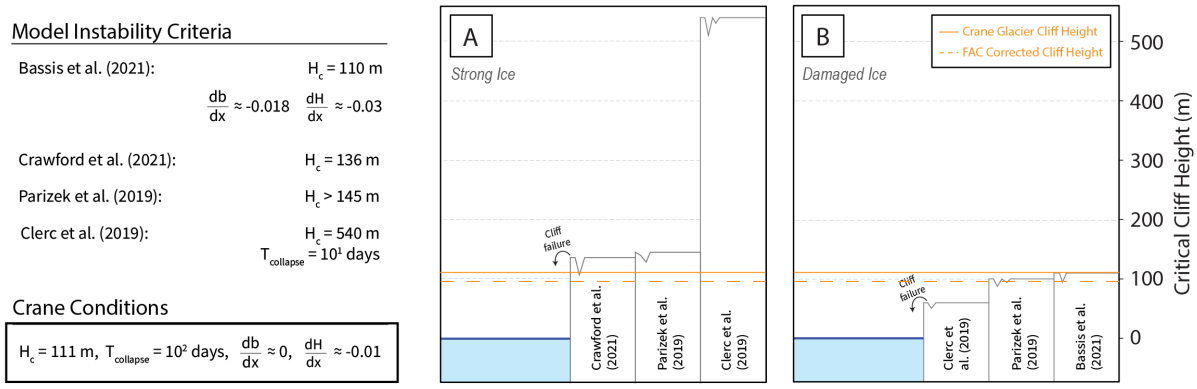

Figure 3. Conditions at Crane Glacier compared to process model predictions of cliff failure thresholds. (Left) Process model criteria required to trigger MICI (see Supplementary Text), including subaerial cliff height (H_c), bed slope ($\frac{db}{dx}$), ice thickness gradient ($\frac{dH}{dx}$), and timescale of ice shelf collapse ($T_{collapse}$), with conditions we observe at Crane Glacier provided. Model instability criteria are upper-bound values resulting from strong/undamaged treatment of ice. (Right) Schematic diagram comparing the cliff heights required for brittle failure under (a) strong and (b) weak model treatment of ice, if included in referenced work.

5 Conclusions

Despite Crane Glacier being invoked in many conversations of unstable ice cliff failure, the limited data collected during the LBIS collapse event cannot unambiguously validate the MICI hypothesis. Previous analysis of Crane Glacier's behavior from 2002-2004 is predicated on an inaccurate 2002 groundingline position, but our analysis shows that retreat in 2002 and 2003 occurred in a remnant, floating ice shelf. Regardless, rapid, unstable terminus retreat dominated in the years following LBIS collapse, highlighting the fact that brittle failure governed Crane Glacier's evolution through 2004. This includes the final phase of retreat, which may have occurred by the failure of a grounded ice cliff with a height of 111 m. Data bounding the final phase of retreat constrain the minimum possible failure rate of this system at ~7.9 km/a.

The glacier terminus retreated to a configuration with stresses at the brittle failure threshold, where continued failure maintained a constant terminus position for 7 years with no further retreat. Meanwhile, the mass dis-equilibrium induced by terminus changes drove widespread thinning in the glacier interior. Finally, as sea-ice filled the fjord in 2011, Crane Glacier's terminus advanced and an ice shelf was re-established, supporting a thickening and slowing (but overall thinner than pre LBIS collapse) glacier profile.

Given a maximum terminal cliff height of only 111 m tall, available process models indicate that terminus stresses would not exceed the yield strength of undamaged ice. However, using realistic but high values for ice damage, and with the corresponding reduction in yield strength, cliff failure at Crane Glacier becomes consistent with the process models discussed here. This highlights the importance of better understanding ice shelf damage in projecting future ice sheet behavior – if high damage is plausible for Crane Glacier, it means that cliff failure likely did govern the final stage of glacier retreat, and future ice sheet margins may be susceptible to brittle failure with cliff heights as low as 60 m, as predicted by Clerc et al. (2019).

The rapid nature of ice shelf break up makes observing ice cliff failure an inherently challenging problem. Brittle processes are fast and therefore require high temporal sampling to observe, best accomplished in situ. Measuring cliff failure processes will require having field sensors in the right place at the right time, something not easily done at scale. This means that observational evaluation of ice cliff models must, in part, rely on the temporally limited (and therefore at times, ambiguous) remote sensing record. While studies like this one cannot end the debate over model realism and the role of cliff failure in the future evolution of the Antarctic Ice Sheet, they contribute to the larger corpus of evidence that will be required to justify the inclusion and treatment of cliffs in continental scale models of Antarctica and Greenland.

Acknowledgments

This work was funded through NASA award 80NSSC20K0958. We would like to thank the Polar Geospatial Center, who provided stereo-pair DEMs generated

from MAXAR imagery over Crane Glacier.

Data Availability Statement

Pre-IceBridge and IceBridge altimetry data, and MEaSUREs velocity data were downloaded from the National Snow and Ice Data Center at: https://nsidc.org/data/BLATM2/versions/1, https://nsidc.org/data/ILATM2/versions/2, and https://nsidc.org/data/NSIDC-0720/versions/1. Velocity data generated using auto-RIFT (Gardner et al., 2018) and provided by the NASA MEaSUREs ITS_LIVE project (Gardner et al., 2019) were downloaded from the following repository: https://github.com/nasa-jpl/its_live. Landsat images were downloaded from https://earthexplorer.usgs.gov. Figures were made with Matplotlib version 3.4.3, available under the Matplotlib license at https://matplotlib.org/.

References

Alley, R. B., Horgan, H. J., Joughin, I., Cuffey, K. M., Dupont, T. K., Parizek, B. R., Anandakrishnan, S., & Bassis, J. (2008). A Simple Law for Ice-Shelf Calving. *Science*, *322*(5906), 1344–1344. https://doi.org/10.1126/science.1162543Ashmore, D. W., Hubbard, B., Luckman, A., Kulessa, B., Bevan, S., Booth, A., Munneke, P. K., O'Leary, M., Sevestre, H., & Holland, P. R. (2017). Ice and firn heterogeneity within Larsen C Ice Shelf from borehole optical televiewing. *Journal of Geophysical Research: Earth Surface*, *122*(5), 1139–1153. https://doi.org/10.1002/2016JF004047Bassis, J. N., Berg, B., Crawford, A. J., & Benn, D. I. (2021). Transition to marine ice cliff instability controlled by ice thickness gradients and velocity. *Science*, *372*(6548), 1342–1344. https://doi.org/10.1126/science.abf6271Bassis, J. N., & Walker, C. C. (2012). Upper and lower limits on the stability of calving glaciers from the yield strength envelope of ice. *Proceedings of the Royal Society A: Mathematical, Physical and Engineering Sciences*, *468*(2140), 913–931. https://doi.org/10.1098/rspa.2011.0422Bell, R. E., Banwell, A. F., Trusel, L. D., & Kingslake, J. (2018). Antarctic surface hydrology and impacts on ice-sheet mass balance. *Nature Climate Change*, *8*(12), 1044–1052. https://doi.org/10.1038/s41558-018-0326-3Blair, J. B., Hofton, M. A., & Rabine, D. L. (2018). *Processing of NASA LVIS elevation and canopy (LGE, LCE and LGW) data products*. http://lvis.gsfc.nasa.govBorstad, C. P., Khazendar, A., Larour, E., Morlighem, M., Rignot, E., Schodlok, M. P., & Seroussi, H. (2012). A damage mechanics assessment of the Larsen B ice shelf prior to collapse: Toward a physically-based calving law. *Geophysical Research Letters*, *39*(18). https://doi.org/10.1029/2012GL053317Bulthuis, K., Arnst, M., Sun, S., & Pattyn, F. (2019). Uncertainty quantification of the multi-centennial response of the Antarctic ice sheet to climate change. *The Cryosphere*, *13*(4), 1349–1380. https://doi.org/10.5194/tc-13-1349-2019Christie, F. D. W., Benham, T. J., Batchelor, C. L., Rack, W., Montelli, A., & Dowdeswell, J. A. (2022). Antarctic ice-shelf advance driven by anomalous atmospheric and sea-ice circulation. *Nature Geoscience*, *15*(5), 356–362. https://doi.org/10.1038/s41561-022-00938-xClerc, F., Minchew, B. M., & Behn, M. D. (2019). Marine Ice Cliff Instability

Mitigated by Slow Removal of Ice Shelves. *Geophysical Research Letters*, *46*(21), 12108–12116. https://doi.org/10.1029/2019GL084183Crawford, A. J., Benn, D. I., Todd, J., Åström, J. A., Bassis, J. N., & Zwinger, T. (2021). Marine ice-cliff instability modeling shows mixed-mode ice-cliff failure and yields calving rate parameterization. *Nature Communications*, *12*(1), 2701. https://doi.org/10.1038/s41467-021-23070-7De Rydt, J., Gudmundsson, G. H., Rott, H., & Bamber, J. L. (2015). Modeling the instantaneous response of glaciers after the collapse of the Larsen B Ice Shelf. *Geophysical Research Letters*, *42*(13), 5355–5363. https://doi.org/10.1002/2015GL064355DeConto, R. M., & Pollard, D. (2016). Contribution of Antarctica to past and future sea-level rise. *Nature*, *531*(7596), 591–597. https://doi.org/10.1038/nature17145Dupont, T. K., & Alley, R. B. (2005). Assessment of the importance of ice-shelf buttressing to ice-sheet flow. *Geophysical Research Letters*, *32*(4). https://doi.org/10.1029/2004GL022024Edwards, T. L., Brandon, M. A., Durand, G., Edwards, N. R., Golledge, N. R., Holden, P. B., Nias, I. J., Payne, A. J., Ritz, C., & Wernecke, A. (2019). Revisiting Antarctic ice loss due to marine ice-cliff instability. *Nature*, *566*(7742), 58–64. https://doi.org/10.1038/s41586-019-0901-4Fang Wang, Bamber, J. L., & Xiao Cheng. (2015). Accuracy and Performance of CryoSat-2 SARIn Mode Data Over Antarctica. *IEEE Geoscience and Remote Sensing Letters*, *12*(7), 1516–1520. https://doi.org/10.1109/LGRS.2015.2411434Fox-Kemper, B., Hewitt, H. T., Xiao, C., Aðalgeirsdóttir, G., Drijfhout, S. S., Edwards, T. L., Golledge, N. R., Hemer, M., Kopp, R. E., Krinner, G., Mix, A., Notz, D., Nowicki, S., Nurhati, I. S., Ruiz, L., Sallée, J.-B., Slangen, A. B. A., & Yu, Y. (2021). Ocean, Cryosphere and Sea Level Change. In V. Masson-Delmott, P. Zhai, A. Pirani, S. L. Connors, C. Péan, S. Berger, N. Caud, Y. Chen, L. Goldfarb, M. I. Gomis, M. Huang, K. Leitzell, E. Lonnoy, J. B. R. Matthews, T. K. Maycock, T. Waterfield, O. Yelekçi, R. Yu, & B. Zhou (Eds.), *Climate Change 2021: The Physical Science Basis. Contribution of Working Group I to the Sixth Assessment Report of the Intergovernmental Panel on Climate Change* (pp. 1211–1362). Cambridge University Press. 10.1017/9781009157896.011Gardner, A. S., Fahnestock, M. A., & Scambos, T. A. (2019). *MEaSUREs ITS_LIVE Landsat Image-Pair Glacier and Ice Sheet Surface Velocities: Version 1.* https://doi.org/10.5067/IMR9D3PEI28UGlasser, N. F., & Scambos, T. A. (2008). A structural glaciological analysis of the 2002 Larsen B ice-shelf collapse. *Journal of Glaciology*, *54*(184), 3–16. https://doi.org/10.3189/002214308784409017Golledge, N. R., Keller, E. D., Gomez, N., Naughten, K. A., Bernales, J., Trusel, L. D., & Edwards, T. L. (2019). Global environmental consequences of twenty-first-century ice-sheet melt. *Nature*, *566*(7742), 65–72. https://doi.org/10.1038/s41586-019-0889-9Helanow, C., Iverson, N. R., Zoet, L. K., & Gagliardini, O. (2020). Sliding relations for glacier slip with cavities over three-dimensional beds. *Geophysical Research Letters*, *47*(3), e2019GL084924.Holland, P. R., Corr, H. F. J., Pritchard, H. D., Vaughan, D. G., Arthern, R. J., Jenkins, A., & Tedesco, M. (2011). The air content of Larsen Ice Shelf. *Geophysical Research Letters*, *38*(10), n/a-n/a. https://doi.org/10.1029/2011GL047245Howat, I.

M., Joughin, I., Tulaczyk, S., & Gogineni, S. (2005). Rapid retreat and acceleration of Helheim Glacier, east Greenland. *Geophysical Research Letters*, *32*(22). https://doi.org/10.1029/2005GL024737Joughin, I., Smith, B. E., & Schoof, C. G. (2019). Regularized Coulomb Friction Laws for Ice Sheet Sliding: Application to Pine Island Glacier, Antarctica. *Geophysical Research Letters*, *46*(9), 4764–4771. https://doi.org/10.1029/2019GL082526Joughin, I., Smith, B. E., Shean, D. E., & Floricioiu, D. (2014). Brief Communication: Further summer speedup of Jakobshavn Isbræ. *The Cryosphere*, *8*(1), 209–214. https://doi.org/10.5194/tc-8-209-2014Kingslake, J., Ely, J. C., Das, I., & Bell, R. E. (2017). Widespread movement of meltwater onto and across Antarctic ice shelves. *Nature*, *544*(7650), 349–352. https://doi.org/10.1038/nature22049Lai, C.-Y., Kingslake, J., Wearing, M. G., Chen, P.-H. C., Gentine, P., Li, H., Spergel, J. J., & van Wessem, J. M. (2020). Vulnerability of Antarctica's ice shelves to meltwater-driven fracture. *Nature*, *584*(7822), 574–578. https://doi.org/10.1038/s41586-020-2627-8Lhermitte, S., Sun, S., Shuman, C., Wouters, B., Pattyn, F., Wuite, J., Berthier, E., & Nagler, T. (2020). Damage accelerates ice shelf instability and mass loss in Amundsen Sea Embayment. *Proceedings of the National Academy of Sciences*, *117*(40), 24735–24741. https://doi.org/10.1073/pnas.1912890117Medley, B., Neumann, T. A., Zwally, H. J., & Smith, B. E. (2020). Forty-year Simulations of Firn Processes over the Greenland and Antarctic Ice Sheets. *The Cryosphere Discussions*, 1–35. https://doi.org/10.5194/tc-2020-266Milillo, P., Rignot, E., Rizzoli, P., Scheuchl, B., Mouginot, J., Bueso-Bello, J. L., Prats-Iraola, P., & Dini, L. (2022). Rapid glacier retreat rates observed in West Antarctica. *Nature Geoscience*, *15*(1), 48–53. https://doi.org/10.1038/s41561-021-00877-zMobasher, M. E., Duddu, R., Bassis, J. N., & Waisman, H. (2016). Modeling hydraulic fracture of glaciers using continuum damage mechanics. *Journal of Glaciology*, *62*(234), 794–804. https://doi.org/10.1017/jog.2016.68Mouginot, J., Scheuchl, B., & Rignot, E. (2017). *MEaSUREs Annual Antarctic Ice Velocity Maps, Version 1.* NASA National Snow and Ice Data Center Distributed Active Archive Center. https://doi.org/10.5067/9T4EPQXTJYW9Oppenheimer, M., Glavovic, B. C., Hinkel, J., van de Wal, R., Magnan, A. K., Abd-Elgawad, A., Cai, R., Cifuentes-Jara, M., Rica, C., DeConto, R. M., Ghosh, T., Hay, J., Islands, C., Isla, F., Marzeion, B., Meyssignac, B., Sebesvari, Z., Biesbroek, R., Buchanan, M. K., … Pereira, J. (2019). *Sea Level Rise and Implications for Low-Lying Islands, Coasts and Communities.*Parizek, B. R., Christianson, K., Alley, R. B., Voytenko, D., Vaňková, I., Dixon, T. H., Walker, R. T., & Holland, D. M. (2019). Ice-cliff failure via retrogressive slumping. *Geology*, *47*(5), 449–452. https://doi.org/10.1130/G45880.1Pritchard, H. D., Ligtenberg, S. R. M., Fricker, H. A., Vaughan, D. G., van den Broeke, M. R., & Padman, L. (2012). Antarctic ice-sheet loss driven by basal melting of ice shelves. *Nature*, *484*(7395), 502–505. https://doi.org/10.1038/nature10968Rack, W., & Rott, H. (2004). Pattern of retreat and disintegration of the Larsen B ice shelf, Antarctic Peninsula. *Annals of Glaciology*, *39*, 505–510. https://doi.org/10.3189/172756404781814005Rebesco, M., Domack, E., Zgur, F., Lavoie, C., Leventer, A., Brachfeld, S., Willmott, V., Halverson, G.,

Truffer, M., Scambos, T., Smith, J., & Pettit, E. (2014). Boundary condition of grounding lines prior to collapse, Larsen-B Ice Shelf, Antarctica. *Science*, *345*(6202), 1354–1358. https://doi.org/10.1126/science.1256697Riel, B., Minchew, B., & Bischoff, T. (2021). Data-Driven Inference of the Mechanics of Slip Along Glacier Beds Using Physics-Informed Neural Networks: Case Study on Rutford Ice Stream, Antarctica. *Journal of Advances in Modeling Earth Systems*, *13*(11), e2021MS002621.Robel, A. A. (2017). Thinning sea ice weakens buttressing force of iceberg mélange and promotes calving. *Nature Communications*, *8*(1), 14596. https://doi.org/10.1038/ncomms14596Scambos, T. A. (2004). Glacier acceleration and thinning after ice shelf collapse in the Larsen B embayment, Antarctica. *Geophysical Research Letters*, *31*(18), L18402. https://doi.org/10.1029/2004GL020670Scambos, T. A., Berthier, E., & Shuman, C. A. (2011). The triggering of subglacial lake drainage during rapid glacier drawdown: Crane Glacier, Antarctic Peninsula. *Annals of Glaciology*, *52*(59), 74–82. https://doi.org/10.3189/172756411799096204Schlemm, T., Feldmann, J., Winkelmann, R., & Levermann, A. (2021). *Stabilizing effect of mélange buttressing on the Marine Ice Cliff Instability of the West Antarctic Ice Sheet* [Preprint]. Ice sheets/Numerical Modelling. https://doi.org/10.5194/tc-2021-238Studinger, M. (2014). *IceBridge ATM L2 Icessn Elevation, Slope, and Roughness, Version 2*. NASA National Snow and Ice Data Center Distributed Active Archive Center. https://doi.org/10.5067/CPRXXK3F39RVThomas, R., & Studinger, M. (2010). *Pre-IceBridge ATM L2 Icessn Elevation, Slope, and Roughness, Version 1*. NASA National Snow and Ice Data Center Distributed Active Archive Center. https://doi.org/10.5067/6C6WA3R918HJWeertman, J. (1974). Stability of the Junction of an Ice Sheet and an ice Shelf. *Journal of Glaciology*, *13*(67).Wise, M. G., Dowdeswell, J. A., Jakobsson, M., & Larter, R. D. (2016). Evidence of marine ice-cliff instability in Pine Island Bay from iceberg-keel plough marks. *Nature*, *550*, 506–510. https://doi.org/10.1038/nature24458Wuite, J., Rott, H., Hetzenecker, M., Floricioiu, D., De Rydt, J., Gudmundsson, G. H., Nagler, T., & Kern, M. (2015). Evolution of surface velocities and ice discharge of Larsen B outlet glaciers from 1995 to 2013. *The Cryosphere*, *9*(3), 957–969. https://doi.org/10.5194/tc-9-957-2015Zoet, L. K., & Iverson, N. R. (2020). A slip law for glaciers on deformable beds. *Science*, *368*(6486), 76–78. https://doi.org/10.1126/science.aaz1183